Article published online: 2025-06-04

CT-Based Texture Analysis in Indeterminate Pediatric Renal and Pararenal Masses

Stuti Chandola[1] Priyanka Naranje[1] Arun Kumar Gupta[1] Aanchal Kakkar[2] Venkat Iyer[2] Maroof Ahmad Khan[3] Manisha Jana[1]

[1] Department of Radiodiagnosis and Interventional Radiology, All India Institute of Medical Sciences, New Delhi, India
[2] Department of Pathology, All India Institute of Medical Sciences, New Delhi, India
[3] Department of Biostatistics, All India Institute of Medical Sciences, New Delhi, India

Address for correspondence Manisha Jana, MD, DNB, FRCR, Department of Radiodiagnosis and Interventional Radiology, All India Institute of Medical Sciences, Ansari Nagar, New Delhi 110029, India (e-mail: manishajana@gmail.com).

Indian J Radiol Imaging 2026;36:76–83.

Abstract

Background Differentiation between pediatric Wilms tumor and neuroblastoma may be difficult when solely based on conventional computed tomography (CT) features, especially in large tumors.

Objective This article analyzes the role of CT-based texture analysis (CTTA) in differentiating (1) pediatric Wilms tumor and neuroblastoma and (2) between histological and *MYCN* amplified subtypes of neuroblastoma.

Materials and Methods Treatment-naive cases of pediatric (< 18 years) renal/pararenal tumors who underwent a single-phase contrast-enhanced CT of chest, abdomen, and pelvis for staging and preoperative evaluation purposes were enrolled. CT images were processed with texture analysis software for first-order texture features. Calculated parameters included mean, variance, skewness, and kurtosis. Grayscale features were also analyzed among the tumor groups and subgroups. Mann–Whitney *U* and Fisher's exact tests were used for statistical analysis. A *p*-value of < 0.05 was considered significant.

Observations and Results A total of 37 lesions (22 neuroblastoma, 15 Wilms) were evaluated. With respect to grayscale features, neuroblastoma tumors exhibited calcifications in greater frequency with a higher propensity for nodal and visceral metastasis. Significant differences were observed when comparing variance of the two tumor groups with neuroblastoma showing higher intralesional variance values than Wilms tumor. Undifferentiated subtype of neuroblastoma demonstrated higher intralesional variance than other two subtypes combined; *MYCN* amplified tumors showed higher intralesional mean value than unamplified tumors ($p < 0.05$ for both). The various neuroblastoma subgroups did not significantly differ when considering the grayscale parameters.

Conclusion CTTA has a potential role in allowing differentiation between neuroblastoma and Wilms tumor. It may additionally allow differentiation among various histological subtypes of neuroblastoma and detection of *MYCN* amplified neuroblastoma.

Keywords
- texture analysis in CT
- pediatric renal masses
- Wilms tumor
- neuroblastoma

article published online
June 4, 2025

DOI https://doi.org/10.1055/s-0045-1808089.
ISSN 0971-3026.

Thieme Medical and Scientific Publishers Pvt. Ltd., A-12, 2nd Floor, Sector 2, Noida-201301 UP, India

Introduction

Renal and pararenal tumors together constitute the most common pediatric abdominal malignancy.[1] While Wilms tumor (WT) remains the most frequently occurring renal tumor, a major differential diagnosis of the same includes neuroblastoma (NB), which typically presents as a pararenal mass.[1,2] Differentiation between renal and pararenal masses is of utmost importance for appropriate surgical planning and outcome. Additionally, parameters allowing distinction between the individual tumor subtypes offer advantages of preoperative prognostication and management.[2] This is particularly pertinent in NB, which is a tumor with diversified clinical outcomes that primarily depend upon the histological subtypes (differentiated [DF], poorly differentiated [PD], and undifferentiated [UD]).[3] Another important genetic marker that prognosticates NB is *MYCN* amplification. Therefore, early identification of such attributes on imaging may contribute to early patient stratification and appropriate protocol assignment at the time of diagnosis.[2]

Various imaging modalities like contrast-enhanced computed tomography (CECT) and CE magnetic resonance imaging (MRI) have been explored in the differentiation of renal and pararenal masses. MRI avoids the risk of ionizing radiation, but is costly with limited availability and is associated with the risks of general anesthesia.[2] CECT can be performed under light anesthesia or sedation and offers decent evaluation of certain features like calcifications; however, it falls short with regards to differentiation between the various masses with subjective visual interpretation of heterogeneity and Hounsfield unit value being the limited options available.[4] Although biopsy remains the gold standard, it is invasive with added burden of cost and morbidity associated with the invasive procedure.

CT-based texture analysis (CTTA) is a form of image processing that reduces subjectivity in image interpretation.[4] This technique potentially provides a quantitative evaluation of region-to-region differences in pixel intensity that may not be detected with the unaided eye.[4,5] They provide numeric descriptors of "heterogeneity." Previous studies have shown there exists quantifiable texture differences between benign and malignant lesions (more heterogeneity in malignant lesions), possibly allowing pathologic differentiation in specific clinical settings.[5] CTTA has thus been referred to as "virtual biopsy" in the literature.[4–6]

Various CT-based texture parameters have been evaluated to differentiate malignant and benign tumors.[4,6–10] Additionally, it has also been evaluated to determine the histology subtype of malignant renal tumors.[5,7]

While texture analysis has been used extensively in adult renal masses, there is a paucity of research utilizing it for pediatric renal masses. Additionally, it is pertinent to consider the diversity within the categories of renal and pararenal tumors common in children when compared to adults, for example, both WT and NB are malignant tumors. Although both may be differentiated on conventional CT, this distinction becomes difficult when considering larger lesions and in situations where the organ of origin is not delineated.

Given this background, the objective of this study was to prospectively analyze the role of CTTA in differentiating the two most common renal and pararenal masses, that is, WT and NB. A secondary objective was to assess the various CT texture parameters that may assist in the differentiation of the histological and genetic subtypes of NB.

Materials and Methods

This prospective observational study was conducted after obtaining the clearance from the institutional ethics committee (IEC No-598/03.07/2020, RP- 39/2020) from October 2020 to September 2022. A written informed consent was obtained for all the patients and guardians (whichever applicable) after explaining the procedure in their vernacular language.

Patient Population

Treatment-naive cases of pediatric ($<$ 18 years) renal/pararenal tumors (diagnosed either on clinical assessment or other imaging modalities) who were referred for staging CT of the abdomen for the purpose of preoperative evaluation were included in the study. Patients who had a prior history of allergy/contraindication to iodinated contrast, who refused to participate, have had chemo- or radiotherapy, and those who underwent biopsy within the last 7 days prior to acquisition were excluded. Eventually, a total of 42 patients were included in the study. This convenient sample was based upon the constraints of the number of patients who presented to the pediatric medicine or pediatric surgery department with renal/perinephric masses and feasibility of investigations.

CT Acquisition

All patients underwent a single-phase CECT of the chest, abdomen, and pelvis on a 128-slice scanner (Somatom Definition AS, Siemens, Erlangen, Germany) acquired 45 seconds following injection of 1.5 mL/kg body weight of an iodinated contrast agent (Omnipaque 300, Iohexol, GE Healthcare, United States) at a rate of 2 to 3.5 mL/s (depending on the intravenous access size) via an automated injector.

The following acquisition parameters were used: 80 kV; AutomA and SmartmA (angular and *z*-axis modulation) using CARE Dose 4D; pitch 1:1; acquisition slice thickness 5 mm; scan field of view (FOV) and display FOV adjusted to patient size. Average CT dose index (CTDI vol) was 4.9 ± 1.9 mGy. The images were reconstructed with a slice thickness of 1 mm in the mediastinal and lung window so as to allow generation of multiplanar reformats for evaluation.

CTTA

We analyzed the first-order histogram-based texture features for differentiating between WT and NB. Histogram-based features were spatially invariant and the arrangement of the pixels relative to one another did not affect the analysis. A commercially available research software MaZda (MaZda package, www.eletel.p.lodz.pl, developed at Technical University of Lodz [TUL], Poland) was utilized for the calculation of the

first-order texture parameters and included a Laplacian of Gaussian spatial filter to remove any spatial heterogeneity seen in the images.[11,12]

Image Analysis

The images were analyzed by a single reader with 12 years of experience in pediatric radiology who was blinded to the clinical and pathological findings.

Analysis of Grayscale Features

The images were analyzed for the following morphological parameters: tumor size, margins, and presence of claw sign (i.e., mass forming sharp angles with the renal parenchyma on either side, implying renal origin) for delineating the organ of origin. Additional features that were evaluated included tumor heterogeneity (i.e., presence of necrosis and/or hemorrhage), presence and nature of calcification (coarse or fine), vascular encasement and infiltration, intraspinal extension, presence of lymphadenopathy, and distant metastasis to the liver, lung, and bones.

Texture Analysis

CT images were transformed into Digital Imaging and Communications in Medicine format and further processed with the free available texture analysis software MaZda. A single axial section that included homogeneous solid component of the tumor, which was free of necrosis and/or calcification, was chosen. A polygonal region of interest (ROI) was drawn by the radiologist on this largest representative axial section within the boundary of the tumor and the texture parameters were saved for each tumor (►**Fig. 1**). Gray-level normalization was performed for each ROI, using the limitation of dynamics to $\mu \pm 3$ standard deviation (SD) (μ gray-level mean) to minimize the influence of contrast and brightness variation, as it was performed in previous studies.[13,14]

The first-order histogram parameters calculated by the automated software and subsequently analyzed included mean (average intensity from the pixels in the examined slice), variance (indicator of spread of individual intensity value(s) from the mean), skewness (measurement of asymmetry in distribution), and kurtosis (measurement of "outlier" or "extreme" pixel values).

Histopathological Evaluation

Histopathological examination was considered the gold standard for diagnosis. Specimens included prechemotherapeutic percutaneous biopsies from the primary tumor or from metastatic sites, and excision specimens for cases undergoing upfront surgery.

Detection of *MYCN* Amplification in Neuroblastomas

MYCN status was assessed by fluorescence in situ hybridization, using a *MYCN/CCP2* dual-color probe set in cases diagnosed as NB. *MYCN* was considered amplified when *MYCN* signals exceeded CCP2 signals by ≥ 3 times or if ≥ 10 *MYCN* signals were present per nucleus.

Statistical Analysis

The demographics, imaging findings, and the various texture parameters obtained from CTTA were recorded in GraphPad Prism version 9.0 software (GraphPad, San Diego, California, United States). Biopsy results were considered the gold standard for analysis. Categorical variables were expressed as frequencies and percentages and continuous variables are expressed as median $\pm$ SDs along with interquartile range. Categorical variables were compared using Fisher's exact and chi-square tests. Continuous variables were compared using the Mann–Whitney *U*/Wilcoxon rank sum and Welch's unpaired t-tests. A p-value of < 0.05 was considered to indicate statistical significance. Receiver operating characteristics (ROC) curve analysis was used to obtain the area under the curve (AUC) for texture parameter(s) found to be significantly different between the various histological groups, and optimal cutoffs were obtained.

Observations and Results

A total of 42 lesions were included in the study and were categorized into three major categories: 22 cases (52.4%) of NB (mean age 3.3 ± 2.5 years), 15 cases (35.7%) with WT

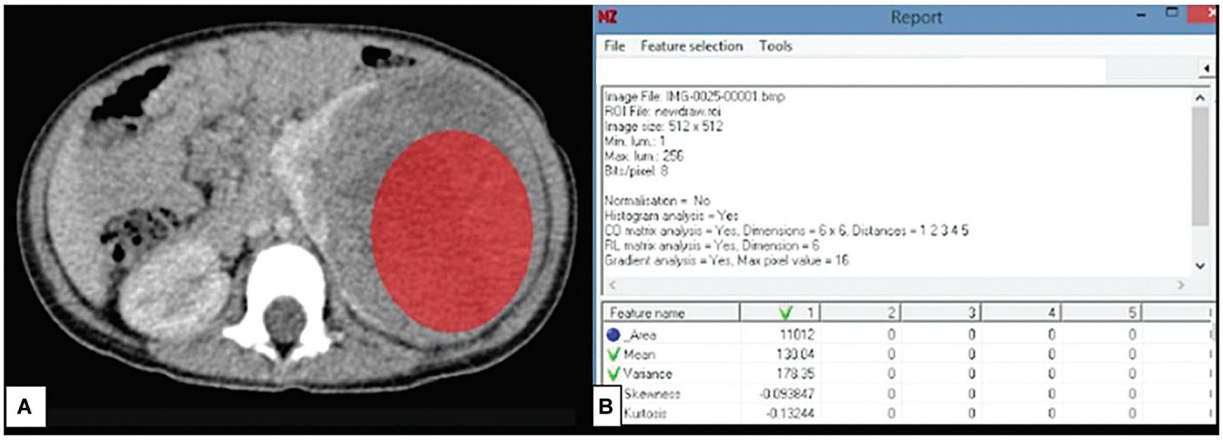

Fig. 1 Assessment of the images using texture analysis software. (**A**) Representative axial section of the tumor. A polygonal region of interest (ROI) was drawn within the boundary of the tumor and texture parameters were calculated for each tumor (**B**). These included mean, variance, skewness, and kurtosis.

(mean age 3.6 ± 1.7 years), and 5 cases (11.9%) with other malignancies. The third category included one case each of the following malignancies—anaplastic large cell lymphoma, anaplastic sarcoma, ganglioneuroblastoma, clear cell sarcoma, and extraosseous Ewing sarcoma. Texture analyses (CTTA) were performed for the first two categories as these were most prevalent in the study population and were feasible for evaluation.

Analysis of Grayscale Features on CECT

No significant difference was observed among the two malignancy groups with respect to the patient age, lesion size (p 0.06), and intralesional heterogeneity (p 0.26). Although a major proportion of tumors in the NB subgroup showed a tendency toward encasing the vessels, this difference was not significant when comparing the two groups (p 0.1). A significant difference was demonstrated among both groups when considering presence of calcifications, with NB exhibiting calcifications in a greater frequency (p 0.007). Although the NB group had a higher tendency to exhibit coarse calcifications, this difference was not significant (►**Fig. 2**). None of the lesions showed intraspinal extension.

Statistically significant differences were observed in the two groups when considering nodal involvement (p 0.04) and visceral metastasis (p 0.007); NB typically showed a greater tendency of nodal, hepatic, and skeletal involvement. WT had a lower frequency of metastasis (13.4% in WT vs. 59.1% in NB) and lung was the only site of distant spread.

Thirteen cases (86.7%) with WT demonstrated a positive claw sign and this was not seen in NB. A particular organ of origin could not be ascertained in four lesions.

CT-Based Texture Analysis Among Two Groups (►Table 1)

A statistically significant difference was observed when comparing the variance of the two tumor groups (p-value < 0.05), with NB showing higher intralesional variance values as compared with the WT subgroups. Such a difference was not demonstrated by other parameters (mean, variance, and skewness).

Neuroblastoma Subgroup Evaluation (►Tables 2 and 3)

Among the cases of NB, histological and genetic subtyping were available for 19 cases; the histological subtyping is as follows: 12 cases (63.15%) of "UD" category, 6 cases with "PD," and 1 case of "DF" subtypes. For analysis, PD and DF categories were pooled together and compared with the UD categories. No significant differences were observed among the grayscale parameters in between the two tumor subgroups.

A statistically significant difference was demonstrated in comparison of the variance of the two subgroups (p-value < 0.05); UD NB exhibited higher intralesional variance than the other categories (►**Table 2**).

MYCN status was available for 19 cases, which were considered for analysis through CTTA. Amplification of the *MYCN* gene was observed in 9 cases (47.3%); none of the grayscale features could aid in differentiation between the two groups, though it was observed that tumors with absence of *MYCN*

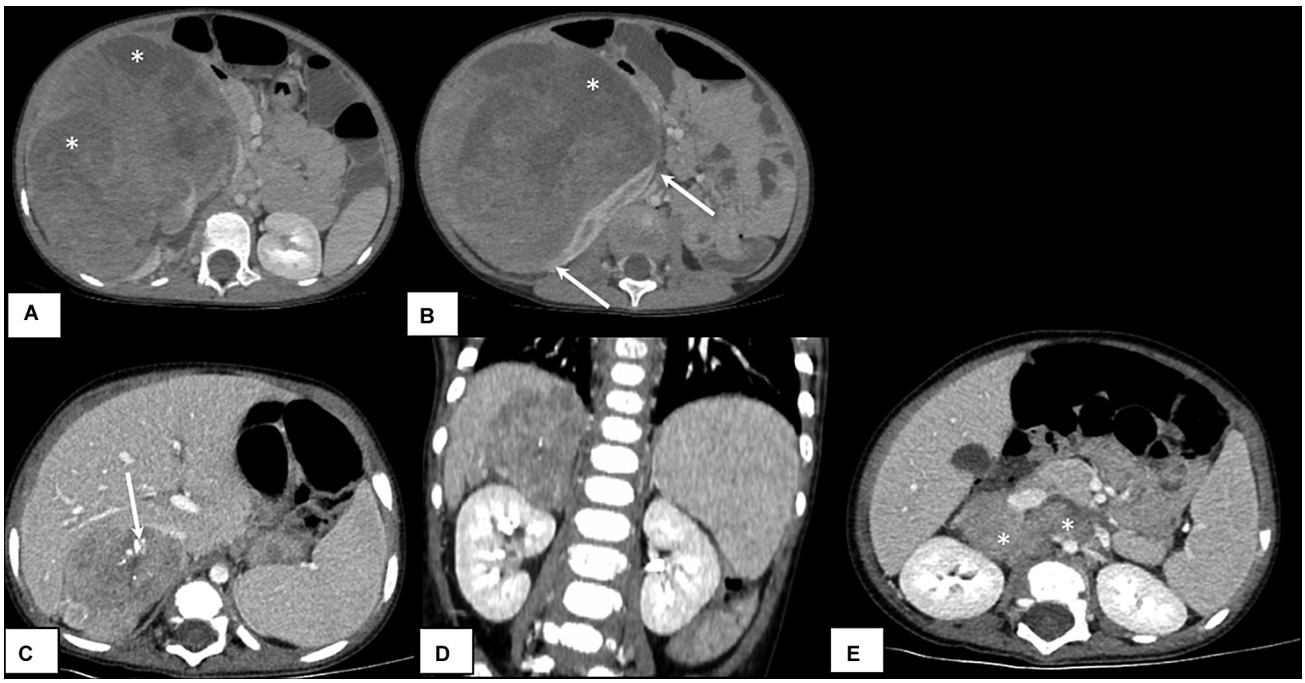

Fig. 2 Grayscale computed tomography (CT) features of Wilms and neuroblastoma. (**A** and **B**) Wilms tumor in a 4-year-old female. Serial axial contrast-enhanced CT (CECT) images show a large heterogeneous mass with necrotic areas within (asterisk, **A** and **B**) in the right side of the abdomen, reaching up to the midline and forming a claw with the right renal parenchyma (arrows, **B**). (**C**–**E**) Neuroblastoma in a 3-year-old male. Axial (**C**) and coronal (**D**) CECT images show an enhancing right suprarenal mass with central calcifications (arrow). Serial axial CECT image (**E**) shows multiple conglomerated retroperitoneal nodes encasing the aorta and bilateral renal arteries (asterisk, **E**).

Table 1 Texture parameters of neuroblastoma and Wilms tumor groups ($n = 37$)

Sl. no.	Feature	Neuroblastoma ($n = 22$) (median ± SD) [interquartile range]	Wilms tumor ($n = 15$) (median ± SD) [interquartile range]	*p*-Value
1.	Mean	149.31 ± 34.11 [129.42–162.72]	130.2 ± 17.73 [126.26–151.56]	0.12
2.	Variance	277.39 ± 230.53 [221.52–469.55]	145.78 ± 89.31 [98.41–253.06]	**0.01**
3.	Skewness	0.05 ± 0.56 [–0.06, 0.29]	0.08 ± 0.17 [–0.04, 0.17]	0.75
4.	Kurtosis	0.30 ± 3.28 [–0.24, 1.07]	–0.01 ± 0.21 [–0.13, 0.23]	0.19

Abbreviation: SD, standard deviation.
Note: Bold highlighted values indicate statistically significant values within the table; the authors intend to highlight these values.

Table 2 Texture parameters among the histological subgroups of neuroblastoma ($n = 19$)

Sl. no.	Feature	Poorly differentiated and differentiating ($n = 7$) (median ± SD) [interquartile range]	Undifferentiated ($n = 12$) (median ± SD) [interquartile range]	*p*-Value
1.	Mean	161.72 ± 16.28 [146.9–170.14]	147.66 ± 38.83 [120.165–160.9]	0.11
2.	Variance	221.52 ± 73.77 [138.98–250.05]	439.08 ± 236.17 [263.315–589.605]	**0.02**
3.	Skewness	0.07 ± 0.24 [–0.16, 0.32]	0.04 ± 0.74 [0.03–0.38]	0.79
4.	Kurtosis	0.36 ± 0.59 [–0..24, 1.07]	0.25 ± 3.01 [–0.21, 1.17]	0.9

Abbreviation: SD, standard deviation.
Note: Bold highlighted values indicate statistically significant values within the table; the authors intend to highlight these values.

Table 3 Texture parameters among *MYCN* amplified and nonamplified neuroblastomas ($n = 19$)

Sl. no.	Feature	*MYCN* amplified ($n = 9$) (median ± SD) [interquartile range]	*MYCN* nonamplified ($n = 10$) (median ± SD) [interquartile range]	*p*-Value
1.	Mean	141.51 ± 41.52 [111.29–146.9]	160.9 ± 13.64 [149.56–166.99]	**0.02**
2.	Variance	434.2 ± 243.44 [255.87–620.45]	235.50 ± 162.04 [114–295.19]	0.06
3.	Skewness	0.32 ± 0.86 [–0.22, 0.29]	0.13 ± 0.22 [0.03–0.32]	0.41
4.	Kurtosis	0.21 ± 3.49 [–0.38, 0.75]	0.34 ± 0.63 [0.02–1.07]	0.51

Abbreviation: SD, standard deviation.
Note: Bold highlighted values indicate statistically significant values within the table; the authors intend to highlight these values.

amplification were more frequently calcified (►**Fig. 3**). On CTTA, *MYCN* amplified tumors demonstrated significantly lower mean values as compared to *MYCN* nonamplified cases (*p*-value 0.02, ►**Table 3**). Additionally, the two subgroups demonstrated differences among the variance; this was, however, not significant (*p*-value 0.06, ►**Table 3**).

ROC Curve Analysis

To determine the diagnostic value of CTTA in differentiating the NB and WT groups, the optimal cutoff value of tumor variance was calculated. A value of 221.5 yielded a sensitivity and specificity of 81.0 and 73.3%, respectively, in distinguishing the two groups, with the area under the ROC curve being 0.77 (►**Fig. 4**).

Similarly, ROC curves were also calculated for differentiating the subtypes of NB. A cutoff intralesional variance value of 272.4 yielded a sensitivity and specificity of 100.0 and 75%, respectively, in distinguishing the histological groups (UD vs. non-UD) with the area under the ROC curve being 0.82 (►**Fig. 4**).

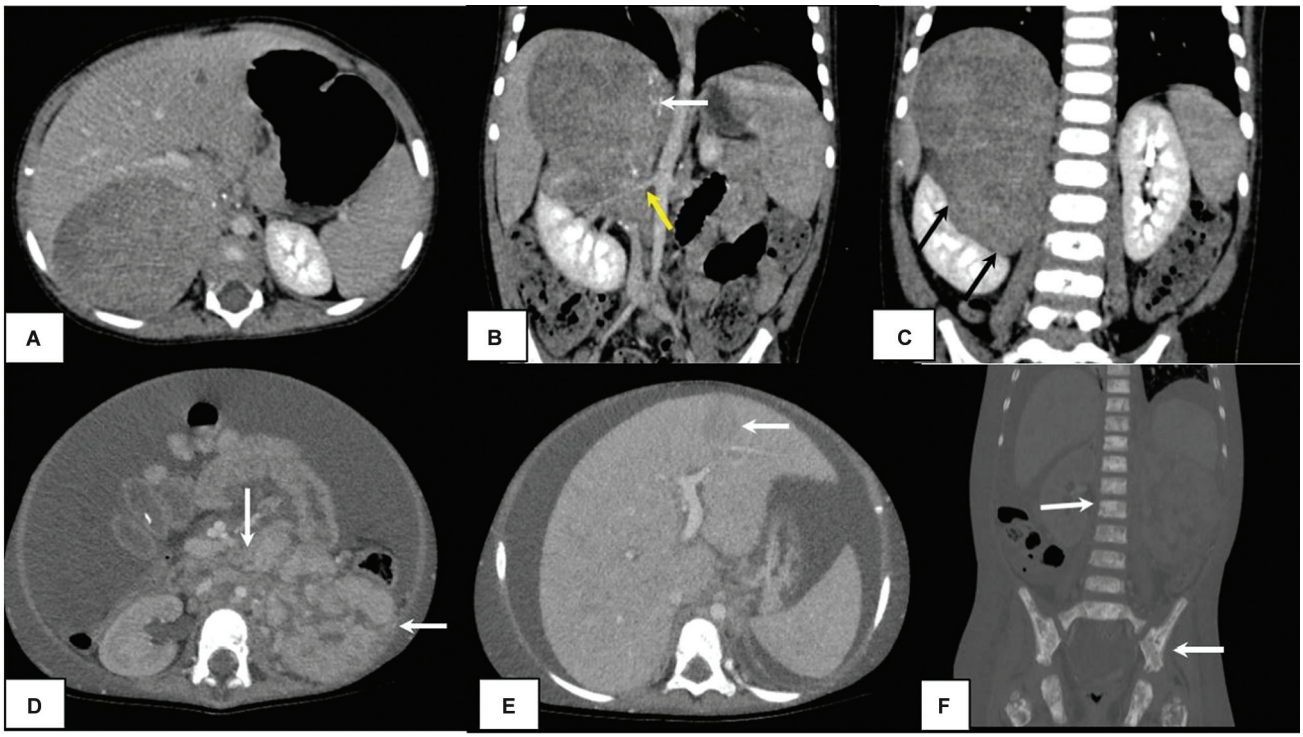

Fig. 3 Grayscale computed tomography (CT) features of subtypes of neuroblastoma. (**A**–**C**) A 2-year-old with differentiated and non-*MYCN* amplified neuroblastoma. Axial (**A**) and serial coronal (**B**, **C**) CT images show a large ovoid homogeneous right suprarenal mass with punctate calcifications (arrow, **B**) displacing and forming dull edges with right kidney (arrow, **C**). The index mass reaches up to the midline with encasement of the right renal artery (yellow arrow, **B**). (**D**–**F**) A 4-year-old with undifferentiated and *MYCN* amplified neuroblastoma. Axial contrast-enhanced CT (CECT) image (**D**) demonstrates an infiltrative necrotic mass infiltrating the entire left kidney with perinephric, contiguous retroperitoneal extension and consequent vascular encasement (arrows, **D**). Gross ascites is seen. Axial CT image at the level of liver (**E**) shows a hypoenhancing metastatic deposit in the left lobe of the liver (arrow, **E**). Coronal image in bone window (**F**) shows multiple sclerotic lesions in the vertebrae and pelvis (arrows, **E**) s/o metastatic involvement.

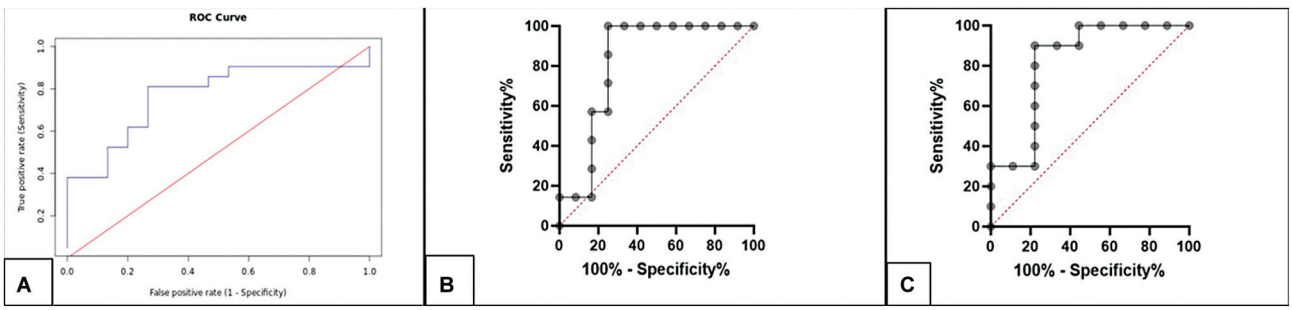

Fig. 4 (A) Receiver operator analysis curve (ROC) for differentiating Wilms tumor and neuroblastoma using variance values on computed tomography (CT)-based texture analysis (CTTA). The area under the curve (AUC) was calculated for ROC curves, and sensitivity and specificity were calculated. AUC was 0.77. (**B**) ROC for differentiating undifferentiated and non-undifferentiated (includes poorly differentiated and differentiated subtypes) histological types of neuroblastoma using variance values on CTTA. AUC was 0.82. (**C**) ROC for differentiating *MYCN* amplified versus nonamplified neuroblastoma using mean values on CTTA. AUC was 0.82.

An intralesional mean value of 148 was able to distinguish *MYCN* amplified from nonamplified tumors with 90% sensitivity and 77.78% specificity; the area under the ROC curve being 0.82 (►**Fig. 4**).

Discussion

NB and WT were the two most common pediatric renal tumors observed in our single-institution study. While WT is the most common malignant pediatric renal tumor, heterogeneity due to convenient sampling may account for the increased number of cases of NB.[2,15] Diversified treatment for both tumors makes it imperative to differentiate between the two, especially on imaging, as tumors of renal origin are candidates for upfront surgery as compared to NB, where neoadjuvant chemotherapy plays an important role especially in advanced categories.[2,3,16] Delineation of the exact organ of origin remains the most important imaging criterion to differentiate among both tumors.

Various imaging features on CT have been used to differentiate the two tumor subgroups and are specially utilized in large tumors where the organ of origin is not delineated. WT tends to show infiltrative margins, with areas of necrosis or hemorrhage within and shows intravascular extension with metastasis to lungs.[15,17] NB, on the other hand, shows homogeneity with coarse calcifications and tends to encase vessels instead of infiltration. We found statistically significant differences between the two subgroups when considering the presence of calcifications and frequency of metastasis. These findings are in agreement with the available literature.[15,16] The rest of the evaluated features did not show a significant difference. Hence, although few grayscale CT features may assist in distinguishing between the two tumor subgroups, they cannot be solely relied upon for accurate differentiation as they lack objectivity. This is especially applicable in large-sized tumors without distant spread.

Texture analysis has been proposed to provide an objective, quantitative assessment of tumor heterogeneity by analyzing the distribution and relationship of voxel gray levels in an image.[7–9,13,14] Different methods of texture analysis have been applied in previous studies, including statistical, model, and transform-based methods.[7–9] Among these, statistical-based techniques have been most commonly applied. In our study, we used first-order statistics, which evaluate the gray-level frequency distribution from the pixel intensity histogram in a given area of interest, including mean intensity, variance or SD, skewness (asymmetry), and kurtosis (peakedness/the flatness of pixel histogram).

On comparing the texture parameters among the two subgroups, we found a significant difference in the variance (p-value < 0.05), with the NB subgroup showing higher intralesional variance values as compared with WT (277.39 ± 230.53 in NB vs. 145.78 ± 89.31 in WT). Other first-order parameters (mean, variance, and skewness) did not demonstrate such differences. Although there are few studies evaluating the texture characteristics of WT on ultrasonography[17] and NB on positron emission tomography /CT and CT,[18,19] there is paucity of literature in the usage of CTTA in differentiation among the two tumor subgroups, which limit the comparison of our observed results. Nevertheless, NB is a tumor characterized by genetic and clinical diversity with unpredictable clinical behaviors, such as spontaneous regression, tumor maturation, and aggressive progression refractory to therapy.[3] The high intralesional variance of the NB group observed in the present study may be representative of the pathological heterogeneity in these tumors. A cutoff value of 221.5 yielded a sensitivity and specificity of 81.0 and 73.3%, respectively, in distinguishing the two groups (AUC 0.77).

NB comprises three different histological subtypes according to the International Neuroblastoma Pathology Committee—UD, PD, and DF.[3] UD subtype tumors are considered as biologically unfavorable, while the majority of DF subtypes are biologically favorable. Tumors in the PD category are intermediate with varying levels of favorability, which is determined by age and mitosis-karyorrhexis index.[3] We combined PD and DF categories for analysis and observed a significant difference on comparison of the variance of the UD and combined PD and DF subgroups (p-value < 0.05), with UD NB exhibiting higher intralesional variance values (439.08 ± 236.17 in UD vs. 221.52 ± 73.77 in combined group). The high variance values may reflect the increased biological aggressiveness of the UD subtype tumors. Our findings are clinically relevant because tumor histology is an important prognostic indicator in NB; hence, early identification of UD tumors is imperative for early intervention of neoadjuvant/adjuvant therapy for improving survival.

MYCN amplification occurs in about 20 to 30% of NBs and confers an adverse prognosis due to aggressive tumor behaviour.[3,20] Irrespective of tumor histology and age, presence of *MYCN* amplification automatically classifies the patient as a high-risk category, which has impact on further management. *MYCN* amplification status was available for 19 patients in our study. Amplification of the gene was observed in 9 cases (47.3%) and these tumors demonstrated significantly lower mean values as compared to *MYCN* nonamplified cases (p-value 0.02). Although *MYCN* amplified tumors also displayed high intralesional variance, this difference (p-value 0.06) fell short of being significant in our study. Few studies are available in preexisting literature where CTTA has been utilized to detect *MYCN* amplification.[20–22] Wu et al suggested that a combined model of radiomics signature and clinical factors held a superior predictive performance in the detection of *MYCN* amplification than using the clinical model alone, with an improved AUC value from 0.82 to 0.95 in the training cohort and 0.70 to 0.91 in their test cohort.[20] However, our study differs from this study as the majority of selected features in radiomics were derived from gray-level run-length matrix, which is a higher-order statistical parameter.

Our study is not without limitations. First, a small number of patients in each tumor group lead to the asymmetric distribution, which could have had an impact on the obtained parameters. This is especially relevant in the differentiation of the histological and molecular subtypes of NB in which three patients could not be included due to unavailability of infrastructure for detecting *MYCN* amplification in the earlier phase of this study. Large-scale prospective studies from multiple institutions are needed for validation before CTTA can be brought in routine practice. Second, we did not calculate second-order and other first-order parameters including threshold (percentage of pixels within a specified range) and entropy (irregularity). First-order histogram analysis does not account for the location of the pixels and lacks any reference to the spatial interrelationship between gray values. Higher-order statistics are calculated using neighborhood gray-tone difference matrices, which examine location and relationships between three or more pixels. Higher-order features therefore have the advantages of evaluating voxels in their local context, taking the relationship with neighboring voxels into account. Additionally, the observed parameters may have been impacted by the software being used and to a lesser extent by the acquisition parameters. Finally, since only one observer evaluated the images and placed the ROIs, therefore, a certain investigator bias cannot be excluded.

Conclusion

CTTA is a useful adjunct to conventional imaging in differentiating between WT and NB, especially in large lesions and situations when the organ of origin is not ascertained. It additionally has a potential value in distinguishing among the various histological subtypes of NB and detection of *MYCN* amplified NB, thereby facilitating patient prognostication and early institution of appropriate treatment in these tumors.

Data Availability Statement

Data can be made available on a reasonable request to the corresponding author.

Authors' Contributions

S.C. collected data, carried out the initial analyses, and drafted the initial manuscript.

M.J. and P.N. conceptualized and designed the study, coordinated and supervised data collection, and critically reviewed and revised the manuscript.

A.G. conceptualized and designed the study, critically reviewed and revised the manuscript for important intellectual content.

A.K. and V.I. supervised the pathological data, critically reviewed and revised the manuscript.

M.A.K. performed the statistical analysis.

All authors approved the final manuscript as submitted and agree to be accountable for all aspects of the work.

Ethical Approval

This prospective observational study was conducted after obtaining the clearance from the institutional ethics committee (IEC No-598/03.07/2020, RP- 39/2020).

Patients' Consent

A written informed consent was obtained for all the patients and guardians after explaining the procedure in their vernacular language.

Funding

None.

Conflict of Interest

None declared.

References

1 Dome JS, Fernandez CV, Mullen EA, et al; COG Renal Tumors Committee. Children's Oncology Group's 2013 blueprint for research: renal tumors. Pediatr Blood Cancer 2013;60(06):994–1000
2 Joseph N, Rai S, Singhal K, et al. Clinico-histopathological profile of primary paediatric intra-abdominal tumours: a multi-hospital-based study. Indian J Surg Oncol 2021;12(03):517–523
3 Shimada H, Ikegaki N. Neuroblastoma pathology and classification for precision prognosis and therapy stratification. In: Neuroblastoma. Academic Press, Cambridge, Massachusetts; 2019:1–22
4 Raman SP, Chen Y, Schroeder JL, Huang P, Fishman EK. CT texture analysis of renal masses: pilot study using random forest classification for prediction of pathology. Acad Radiol 2014;21(12):1587–1596
5 Hodgdon T, McInnes MD, Schieda N, Flood TA, Lamb L, Thornhill RE. Can quantitative CT texture analysis be used to differentiate fat-poor renal angiomyolipoma from renal cell carcinoma on unenhanced CT images? Radiology 2015;276(03):787–796
6 Lubner MG, Stabo N, Abel EJ, Del Rio AM, Pickhardt PJ. CT textural analysis of large primary renal cell carcinomas: pretreatment tumour heterogeneity correlates with histologic findings and clinical outcomes. AJR Am J Roentgenol 2016;207(01):96–105
7 Yu H, Scalera J, Khalid M, et al. Texture analysis as a radiomic marker for differentiating renal tumors. Abdom Radiol (NY) 2017;42(10):2470–2478
8 Feng Z, Shen Q, Li Y, Hu Z. CT texture analysis: a potential tool for predicting the Fuhrman grade of clear-cell renal carcinoma. Cancer Imaging 2019;19(01):6
9 Lubner MG, Smith AD, Sandrasegaran K, Sahani DV, Pickhardt PJ. CT texture analysis: definitions, applications, biologic correlates, and challenges. Radiographics 2017;37(05):1483–1503
10 Kim NY, Lubner MG, Nystrom JT, et al. Utility of CT texture analysis in differentiating low attenuation renal cell carcinoma from cysts: a bi-institutional retrospective study. AJR Am J Roentgenol 2019;213(06):1259–1266
11 Strzelecki M, Szczypinski P, Materka A, Klepaczko A. A software tool for automatic classification and segmentation of 2D/3D medical images. Nucl Instrum Methods Phys Res A 2013;702:137–140
12 Szczypiński PM, Strzelecki M, Materka A, Klepaczko A. MaZda–the software package for textural analysis of biomedical images. In: Computers in Medical Activity. Berlin, Heidelberg: Springer; 2009:73–84
13 Meyer HJ, Schob S, Höhn AK, Surov A. MRI texture analysis reflects histopathology parameters in thyroid cancer - a first preliminary study. Transl Oncol 2017;10(06):911–916
14 Meyer HJ, Leonhardi J, Höhn AK, et al. CT texture analysis of pulmonary neuroendocrine tumors-associations with tumor grading and proliferation. J Clin Med 2021;10(23):5571
15 Chung EM, Graeber AR, Conran RM. Renal tumours of childhood: radiologic-pathologic correlation part 1. The 1st decade: From the radiologic pathology archives. Radiographics 2016;36(02):499–522
16 Watson T, Oostveen M, Rogers H, Pritchard-Jones K, Olsen Ø The role of imaging in the initial investigation of paediatric renal tumours. Lancet Child Adolesc Health 2020;4(03):232–241
17 Shin HJ, Kwak JY, Lee E, et al. Texture analysis to differentiate malignant renal tumours in children using gray-scale ultrasonography images. Ultrasound Med Biol 2019;45(08):2205–2212
18 Feng L, Yang X, Lu X, et al. ^{18}F-FDG PET/CT-based radiomics nomogram could predict bone marrow involvement in pediatric neuroblastoma. Insights Imaging 2022;13(01):144
19 Feng L, Qian L, Yang S, et al. Clinical parameters combined with radiomics features of PET/CT can predict recurrence in patients with high-risk pediatric neuroblastoma. BMC Med Imaging 2022;22(01):102
20 Wu H, Wu C, Zheng H, et al. Radiogenomics of neuroblastoma in pediatric patients: CT-based radiomics signature in predicting MYCN amplification. Eur Radiol 2021;31(05):3080–3089
21 Tan E, Merchant K, Kn BP, et al. CT-based morphologic and radiomics features for the classification of MYCN gene amplification status in pediatric neuroblastoma. Childs Nerv Syst 2022;38(08):1487–1495
22 Chen X, Wang H, Huang K, et al. CT-based radiomics signature with machine learning predicts MYCN amplification in pediatric abdominal neuroblastoma. Front Oncol 2021;11:687884

